Available online at www.sciencedirect.com
SCIENCE DIRECT®
Surface Science 554 (2004) L95–L100
SURFACE SCIENCE
www.elsevier.com/locate/susc

Surface Science Letters

Model-independent X-ray imaging of adsorbed cations at the crystal–water interface

Z. Zhang [a,b], P. Fenter [a,*], L. Cheng [a], N.C. Sturchio [a,c], M.J. Bedzyk [a,b], M.L. Machesky [d], D.J. Wesolowski [e]

[a] *Environmental Research Division, Argonne National Laboratory, ER-203, 9700 South Cass Avenue, Argonne, IL 60439, USA*
[b] *Institute for Environmental Catalysis, Northwestern University, Evanston, IL 60208, USA*
[c] *University of Illinois at Chicago, Chicago, IL 60607, USA*
[d] *Illinois Water Survey, Champaign, IL 61820, USA*
[e] *Oak Ridge National Laboratory, Oak Ridge, TN 37831, USA*

Received 21 October 2003; accepted for publication 12 November 2003

Abstract

We describe an approach to directly image three-dimensional elemental distributions at the crystal–liquid interface with ~1 Å spatial resolution. This method, based on the Fourier synthesis of X-ray standing wave data, is demonstrated by imaging the distribution of Sr^{2+}, Zn^{2+} and Y^{3+} adsorbed to the rutile (1 1 0)-water interface with no a priori assumptions. The approach resolves distinct sites and is robust for systems with single or multiple simultaneous adsorption sites. The observed ion distributions reveal unexpected differences in the adsorption sites of these cations that are needed to interpret electrical double-layer phenomena using surface complexation models.
Published by Elsevier B.V.

Keywords: X-ray standing waves; Solid–liquid interfaces; Adatoms; Surface electronic phenomena (work function, surface potential, surface states, etc.); Titanium oxide

Direct knowledge of solid–liquid interface structure is critically needed to understand many natural and technological processes [1]. The spontaneous accumulation of ions at the oxide–water interface, one manifestation of the widely studied electrical double layer (EDL) [1,2], can be described as a partitioning of EDL ions between the Stern (adsorbed) and Gouy-Chapman (diffuse) layers controlled by specific interactions between the solute ion and the oxide surface. While modern surface complexation models incorporate such site-specific interactions [3–6], the lack of direct knowledge concerning Stern layer structure substantially impedes a fundamental understanding of EDL phenomena.

The ability to *directly* observe cation adsorption sites at the oxide–liquid interface is strongly limited. The development of holographic techniques in recent years has garnered broad interest with

* Corresponding author. Tel.: +1-630-252-7053; fax: +1-630-252-7415.
E-mail address: fenter@anl.gov (P. Fenter).

0039-6028/$ - see front matter Published by Elsevier B.V.
doi:10.1016/j.susc.2003.11.047

their ability to provide model-independent images of atomic structures [7–9]. Yet existing holographic techniques have characteristics that make them inappropriate for imaging atomic distributions at the solid–liquid interface: electron holographies cannot probe the solid–liquid interfaces and X-ray holographies do not yet have the sensitivity to probe interfacial structures. Even the more widely used scanning probe microscopies are limited for systems having non-conducting substrates and they lack elemental specificity [10].

Here, we describe an approach to *directly* image three-dimensional (3D) elemental distributions of cations at the crystal–liquid interface. Imaging distributions in a crystallographic approach relies upon direct measurements of amplitude and phase for each Fourier component, and it has long been recognized that these quantities are probed by the X-ray standing wave (XSW) technique [11,12]. What distinguishes the present results from previous XSW studies of interface adsorption is the *model-independent* derivation of elemental distributions by Fourier synthesis of XSW data using a suitably complete set of Bragg reflections. This new imaging capability makes full use of the elemental and phase-sensitive characteristics of the XSW method [11,12] to reveal adsorbate structures as a phase-sensitive crystallography by projecting the element specific profiles into the substrate unit cell. 3D images of elemental distributions are obtained with a spatial resolution of $\sim$1 Å with no a priori assumptions concerning the elemental distributions (i.e., giving model-independent results). This is a significant improvement upon the traditional analysis of XSW data that relied on comparison of measured and model-calculated quantities. The feasibility of this XSW imaging approach at the crystal–fluid interface is demonstrated through measurements of Sr^{2+}, Zn^{2+}, and Y^{3+} adsorbed at the interface between aqueous solutions and the (1 1 0) surface of rutile (α-TiO_2). Details of experimental procedures and solution conditions are described elsewhere [13].

An XSW is formed by coherent superposition of incident and Bragg-reflected X-ray beams (Fig. 1a), both above and below the surface of a perfect (or nearly perfect) crystal [14,15]. Measurements of characteristic X-ray induced emissions (e.g., X-ray fluorescence) as a function of incident angle at the $\boldsymbol{H} = hkl$ Bragg reflection (with Bragg plane spacing d_H) reveals the Hth Fourier coefficient, $\mathscr{F}_H$, of the element-specific normalized density profile, $\rho(\mathbf{r})$ (including both its amplitude, f_H, and

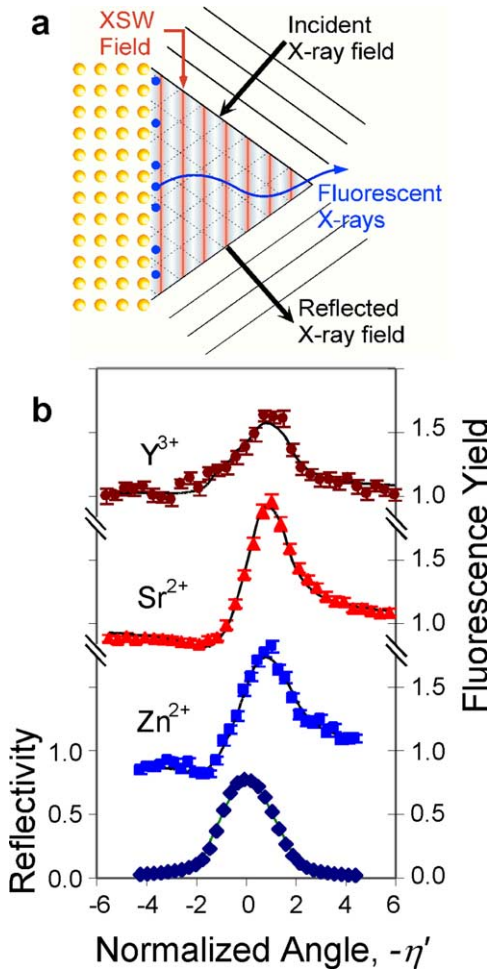

Fig. 1. (a) Schematic of the XSW technique, showing X-ray standing wave (in red) as the coherent sum of the incident and reflected X-ray fields. The fluorescing atoms (in blue) and substrate lattice (in yellow) are also shown. (b) Representative XSW data including substrate Bragg reflectivity and Kα fluorescence data for Y^{3+}, Sr^{2+} and Zn^{2+} using rutile (1 1 0) reflection are shown as a function of the normalized angle parameter $-\eta'$ (incident angle, θ, increases from left to right in plot). X-ray fluorescence is measured with a germanium solid-state detector using dead-time corrections and using suitably detuned Si post-monochromator crystals to match the incident beam dispersion to the selected Bragg reflections.

phase, P_H, also referred to as the coherent fraction and position, respectively). That is, $\mathscr{F}_H = \int \rho(\mathbf{r}) \exp(\mathrm{i}2\pi \boldsymbol{H} \cdot \mathbf{r})\, \mathrm{d}\mathbf{r} = f_H \exp(\mathrm{i}2\pi P_H)$ [11,12].

Cations Sr^{2+}, Zn^{2+}, and Y^{3+} specifically adsorb at the interface between rutile single-crystal (1 1 0) surfaces and aqueous electrolyte solutions (at 25 °C, with pH ~ 6 to 11 and $[Me^{z+}]_{aq} < 10^{-4}$ M), as evidenced by the coherent modulation of the Kα X-ray fluorescence at the (1 1 0) rutile Bragg reflection (Fig. 1b). Coherent positions and fractions for each reflection, determined through comparison of the angular variation of the Bragg reflectivity and X-ray fluorescence signals with calculations using dynamical diffraction theory (shown as lines in Fig. 1b), are listed in Table 1. This analysis does not impose any assumptions on the derived structure since it relies only on information about the substrate crystal structure and the incident X-ray beam properties, with no a priori knowledge concerning the ion distribution. XSW data for adsorbates are traditionally interpreted using a triangulation approach. The adatom location is determined by the intersection of multiple non-colinear planes, each representing a constraint on the adatom location derived from a particular Bragg reflection. However, such an approach is complicated when one or more of the measured coherent fractions is smaller than expected (e.g., see $f_{2\,0\,0}$ for Zn, and $f_{1\,0\,1}$ and $f_{2\,1\,1}$ for Sr in Table 1 the low value of $f_{1\,1\,1}$ for Ti is expected and is a result of phase cancellation between Ti atoms at this reflection). This is indicative of a non-trivial elemental distribution that normally must be understood through comparison of measured and model-calculated values of f_H and P_H.

Table 1
Measured Fourier coefficients of the elemental distributions

d_H		Zn	Sr	Y	Ti
3.25	$P_{1\,1\,0}$	0.95(2)	0.93(2)	0.83(2)	0.99(1)
	$f_{1\,1\,0}$	0.45(3)	0.53(2)	0.36(3)	0.95(1)
2.19	$P_{1\,1\,1}$	0.60(3)	0.93(3)	0.86(2)	0.76(1)
	$f_{1\,1\,1}$	0.31(2)	0.39(3)	0.50(3)	0.17(2)
2.30	$P_{2\,0\,0}$	0.89(4)	0.53(4)	0.35(3)	0.99(1)
	$f_{2\,0\,0}$	0.16(4)	0.36(6)	0.36(8)	0.82(1)
2.49	$P_{1\,0\,1}$	0.91(2)	0.45(8)	–	0.90(1)
	$f_{1\,0\,1}$	0.32(2)	0.09(3)	–	0.99(1)
1.69	$P_{2\,1\,1}$	0.89(2)	0.66(5)	0.34(9)	0.99(1)
	$f_{2\,1\,1}$	0.38(3)	0.11(5)	0.07(5)	0.88(1)
Θ		0.25	0.42	0.12	–

Measured coherent positions, P_H, and fractions, f_H, used to create the XSW images shown in Fig. 2, with estimated uncertainty of last digit in parentheses. Also shown are the Bragg plane spacing d_H (in Å) and the cation Stern-layer coverage Θ in ML (1 ML = 8.8 μmol/m^2), estimated as the product of the total EDL ion coverage and the coherent fraction for the (1 1 0) reflection, $f_{1\,1\,0}$ (the so-called coherent coverage). Absolute ion coverages are determined by comparison to previously calibrated ion-implanted standards.

In the XSW imaging approach, the full elemental distribution, $\rho(\mathbf{r})$, is obtained simply and directly by Fourier inversion of the XSW-measured Fourier coefficients:

$$\rho(\mathbf{r}) = \mathrm{Re}[\Sigma_H \mathscr{F}_H \exp(-2\pi \mathrm{i} \boldsymbol{H} \cdot \mathbf{r})]$$

$$= \mathrm{Re}[\Sigma_H f_H \exp(2\pi \mathrm{i}(P_H - \boldsymbol{H} \cdot \mathbf{r}))]. \quad (1)$$

This approach is robust as long as a sufficiently complete set of $\mathscr{F}_H$ coefficients is measured by XSW. This principle was recently established in the measurement of one-dimensional impurity distributions within a bulk crystal lattice [16]. This has also been applied to a UHV surface adsorbate phase [17]. Such images cannot be simply generated by conventional diffraction techniques (e.g., surface X-ray diffraction) because the phases, P_H, are not directly measured (the so-called 'phase problem' in crystallography).

Full 3D model-independent images of the elemental distributions are obtained with Eq. (1) with the measured coherent fractions and positions in Table 1, making use of the rutile (1 1 0) surface symmetry for symmetry-equivalent reflections. In these images, the derived density profile is shown as a color map. Slices through the derived 3D distributions at the plane of maximum density are shown for Ti (from the substrate crystal) and the adsorbed ions (Fig. 2) to emphasize the ability to determine the adsorbate site. For example, the derived Ti distribution clearly shows two locations within the surface unit cell corresponding to Ti directly bonded to bridging oxygen (BO) sites along [0 0 1] and Ti directly below the terminal oxygen (TO) in the Ti–O plane (see Fig. 2e–g for perspective views of the rutile (1 1 0) unit cell). In

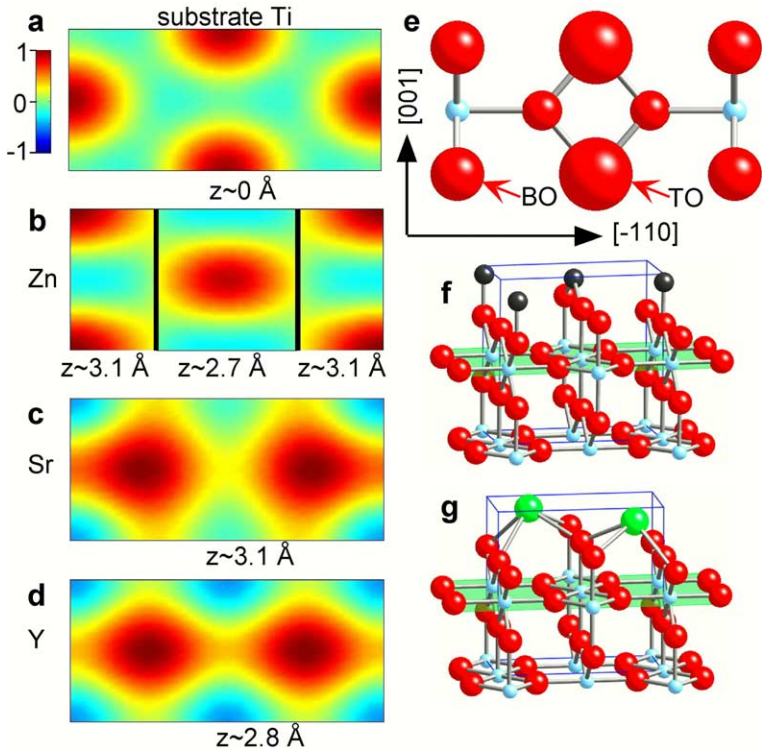

Fig. 2. (a–d) Measured lateral distributions of Ti (from the TiO_2 substrate), and cations Zn^{2+}, Sr^{2+} and Y^{3+} adsorbed to rutile shown as a cut through the plane of maximum density (whose height above the Ti–O plane is indicated below each image) (scale bar shown as inset in panel (a)). (e) Schematic perspective view from above the rutile surface unit cell (oxygen in red, titanium in blue) with BO and TO rows (at heights of 1.265 and 1.983 Å above the Ti–O plane, respectively) along the [0 0 1] direction. Schematic adsorption geometries are shown for (f) Zn and (g) Sr and Y in perspective three-dimensional views of the rutile-water interface. The Ti–O plane is shaded green in (f–g) showing Ti atoms between BOs and directly below each TO.

this approach, images of cation distributions are determined in a similar fashion and are directly referenced to the substrate lattice. These images reveal that Sr^{2+} and Y^{3+} are adsorbed at a "tetradentate" site between two terminal oxygen sites (TO) and two bridging oxygen sites (BO), with differences in their heights controlled primarily by ion radii. In contrast, Zn^{2+} is adsorbed at two distinct sites (each at a different height), primarily above a single BO and to a lesser extent in a bidentate adsorption site between TOs. These Zn^{2+} sites are both close to the projected Ti lattice sites and therefore can be qualitatively understood as due to the similarity of Zn and Ti ionic radii.

These data indicate that the Stern layer distributions are under crystallographic control by the substrate lattice, and reveal two potential difficulties of interpreting ion adsorption phenomena in the absence of such structural information: (1) the unexpected difference in adsorption site for two divalent metals, Sr^{2+} and Zn^{2+}, and (2) the similar adsorption sites for Sr^{2+} and Y^{3+}, even though Sr^{2+} and Y^{3+} are weakly and strongly bound, respectively (as indicated by their differing sensitivity to the concentration of indifferent background electrolytes [13]), and have very different bare ionic radii. Such independent structural information is needed to interpret EDL phenomena using surface complexation models [13].

An important aspect of this XSW imaging approach is its spatial resolution. As is immediately evident from the images in Fig. 2, the resolution obtained from these data is more than sufficient to resolve the various sites. In fact, the intrinsic res-

olution of this approach corresponds to $d_{H_{max}}/2$, where H_{max} is the highest order reflection in Eq. (1) along a particular direction, $\boldsymbol{H}$ [16], so that the present data provide a full 3D image of the ion distributions with a resolution of ~1 Å. The derived Ti distribution is dominated by the experimental resolution, indicated by the largely isotropic distribution in Fig. 2a, as expected since the experimental resolution is substantially larger than the Ti atom vibrational amplitude (<0.1 Å). In contrast, the adsorbate distributions exhibit some additional broadening (e.g., along [0 0 1] for Sr and [−1 1 0] for Zn) suggesting that the actual distributions may include either static or dynamic displacements from the nominal adsorption sites described above. More precise information concerning the adsorbate locations can be obtained by XSW triangulation [15] using the ion adsorption sites in Fig. 2 as a model-independent starting point for a quantitative comparison of measured and calculated f_H and P_H. This model-dependent analysis yields the relative coverage of Zn^{2+} in the two distinct adsorption sites and reveals that both Zn^{2+} species are displaced from their nominal high-symmetry adsorption sites [13].

The Bragg-XSW approach used here is usually assumed to be applicable only to a few select materials that can be grown as perfect crystals (e.g., silicon, germanium). In contrast, the present XSW measurements were performed with imperfect synthetic rutile crystals that would normally be considered inappropriate for XSW analysis, but are made feasible with recent advances in high brilliance X-ray sources that can illuminate small (~100 μm in cross-section) coherently scattering volumes with sufficient flux to retain sub-monolayer sensitivity. The present results demonstrate that XSW-based measurements, including the imaging approach described here, are now applicable to probe reactions at a far broader range of solid–liquid interface systems than previously thought to be possible.

Bragg-XSW images of surface adsorbed species, described here, project 3D ion distributions into the primitive substrate crystallographic unit cell, and therefore emphasize the Stern ion locations over the diffuse ion distribution (because the Debye length is substantially larger than unit cell dimensions). This also results in the well-known modulo-d_H ambiguity in the derived adsorbate position [11,12]. The present results therefore do not distinguish if the adsorbate is, for instance, adsorbed directly to the surface (as an "inner-sphere" adsorbate), or above the surface plane (e.g., either as an "outer-sphere adsorbate" or in the diffuse layer). This inner- vs. outer-sphere ambiguity can be resolved only with additional information (e.g., independent knowledge of ion-substrate interactions, X-ray reflectivity data, molecular dynamics simulations). In this case, the close agreement between XSW results and molecular dynamics simulations demonstrate that each measured adsorbate species occurs as an inner-sphere adsorbate bonding directly to the rutile surface lattice [13]. Bond lengths between adsorbed ions and surface oxygens can be inferred by constraining the positions of surface oxygen atoms with X-ray reflectivity [13] or through analysis of X-ray absorption fine structure data [18,19].

This new model-independent image-based analysis of XSW data is especially important for understanding complex ion distributions. This is illustrated, in this case, by its ability to directly resolve the two distinct Zn^{2+} adsorption sites in a manner that is no more difficult than determining the substrate atom locations or the simpler distributions for Sr^{2+} and Y^{3+}. In systems where there may be co-adsorption of two or more species (e.g., ternary sorption complexes), the elemental sensitivity of XSW allows the distributions of each element to be determined in the same manner as that described above as long as those elements are spectroscopically resolved (e.g., by their respective characteristic emissions).

Extensions of this XSW imaging approach to larger-scale distributions that extend beyond the dimensions of typical substrate crystallographic unit cells can, in principle, be accomplished with other variations of the XSW technique that employ standing waves with longer periods (e.g., through total external reflection or reflection from layered synthetic multilayers [20]), thereby allowing characterization of structures that extend >100 Å from the oxide–water interface. Therefore a complete and direct determination of elemental distributions at the liquid-solid interface can also be

SURFACE SCIENCE LETTERS

achieved for various phenomena with distributions that have defied largely direct characterization, ranging from the diffuse layer distributions in the EDL and ion incorporation in membranes.

Acknowledgements

The authors thank the US Department of Energy, Office of Basic Energy Sciences, Division of Chemical Sciences, Geosciences, and Biosciences, for support of this research. Work was performed at the Advanced Photon Source (beamline 12-ID-D, BESSRC-CAT) and the National Synchrotron Light Source (beamline X15A), which are supported by the US Department of Energy.

References

[1] G.E. Brown Jr. et al., Chem. Rev. 99 (1999) 77.
[2] J. Lyklema, in: Fundamentals of Interface and Colloid Science, vol. II, Academic Press, New York, 1995.
[3] T. Hiemstra, W.H. van Riemsdijk, J. Colloid Interf. Sci. 179 (1996) 488.
[4] M.L. Machesky, D.J. Wesolowski, D.A. Palmer, M.K. Ridley, J. Colloid Interf. Sci. 239 (2001) 314.
[5] D.A. Sverjensky, Geochim. Cosmochim. Acta 65 (2001) 3643.
[6] R.O. James, T.W. Healy, J. Colloid Interf. Sci. 40 (1972) 65.
[7] S. Omori, Y. Nihei, E. Rotenberg, J.D. Denlinger, S. Marchesini, S.D. Kevan, B.P. Tonner, M.A. Van Hove, C.S. Fadley, Phys. Rev. Lett. 88 (1–4) (2002) 055504.
[8] T. Gog, P.M. Len, G. Materlik, D. Bahr, C.S. Fadley, C. Sanchez-Hanke, Phys. Rev. Lett. 76 (1996) 3132.
[9] M. Tegze, G. Faigel, Nature 380 (1996) 49.
[10] R.J. Hamers, J. Phys. Chem. 100 (1996) 13103.
[11] J. Zegenhagen, Surf. Sci. Rep. 18 (1993) 199, and references therein.
[12] M.J. Bedzyk, L. Cheng, Rev. Mineral. Geochem. 49 (2002) 221, and references therein.
[13] Z. Zhang et al., Langmuir (2004), in press.
[14] B.W. Batterman, Phys. Rev. Lett. 22 (1969) 703.
[15] J.A. Golovchenko, J.R. Patel, D.R. Kaplan, P.L. Cowan, M.J. Bedzyk, Phys. Rev. Lett. 49 (1982) 560.
[16] L. Cheng, P. Fenter, M.J. Bedzyk, N.C. Sturchio, Phys. Rev. Lett. 90 (1–4) (2003) 255503.
[17] J.S. Okasinski, D.A. Walko, C.-Y. Kim, M.J. Bedzyk, Phys. Rev. B 69 (2004) 041401(R).
[18] K.F. Hayes, A.L. Roe, G.E. Brown Jr., K.O. Hodgson, J.O. Leckie, G.A. Parks, Science 238 (1987) 783.
[19] P. Fenter, L. Cheng, S. Rihs, M. Machesky, M.J. Bedzyk, N.C. Sturchio, J. Colloid Interf. Sci. 225 (2000) 154.
[20] M.J. Bedzyk, G.M. Bommarito, M. Caffrey, T.L. Penner, Science 248 (1990) 52.